Title

Irreversible Electroporation Combined with Checkpoint Blockade and TLR7 Stimulation Induces Antitumor Immunity in a Murine Pancreatic Cancer Model



Journal

Cancer Immunology Research, 7(10)

ISSN

2326-6066

Authors

Narayanan, Jayanth S Shankara
Ray, Partha
Hayashi, Tomoko
et al.

Publication Date

2019-10-01

DOI

10.1158/2326-6066.cir-19-0101

Peer reviewed

HHS Public Access

Author manuscript

*Cancer Immunol Res*. Author manuscript; available in PMC 2020 April 01.

Published in final edited form as:

*Cancer Immunol Res*. 2019 October ; 7(10): 1714–1726. doi:10.1158/2326-6066.CIR-19-0101.

# Irreversible Electroporation Combined with Checkpoint Blockade and TLR7 Stimulation Induces Anti-Tumor Immunity in a Murine Pancreatic Cancer Model

**Jayanth S. Shankara Narayanan**[1], **Partha Ray**[1], **Tomoko Hayashi**[1], **Thomas C. Whisenant**[3], **Diego Vicente**[1], **Dennis A. Carson**[1], **Aaron M. Miller**[2], **Stephen P. Schoenberger**[2], **Rebekah R. White**[1]

[1]Moores Cancer Center, University of California San Diego, CA

[2]La Jolla Institute of Allergy and Immunology, CA

[3]Department of Computational Biology, University of California San Diego, CA.

## Abstract

Irreversible electroporation (IRE) is a non-thermal ablation technique that is used clinically in selected patients with locally advanced pancreatic cancer, but most patients develop recurrent distant metastatic disease. We hypothesize that IRE can induce an *in situ* vaccination effect by releasing tumor neoantigens in an inflammatory context. Using an immunocompetent mouse model, we demonstrated that IRE alone produced complete regression of subcutaneous tumors in approximately 20%−30% of mice. IRE was not effective in immunodeficient mice. Mice with complete response to IRE demonstrated prophylactic immunity and remained tumor-free when rechallenged with secondary tumors on the contralateral flank. $CD8^+$ T-cells from IRE-responsive mice were reactive against peptides representing model inherent alloantigens and conferred protection against tumor challenge when adoptively transferred into immunocompromised, tumor-naïve mice. Combining IRE with intratumoral toll-like receptor-7 (TLR7) agonist (1V270) and systemic anti-programmed death-1 receptor (PD)-1 checkpoint blockade resulted in improved treatment responses. This combination also resulted in elimination of untreated concomitant distant tumors (abscopal effects), an effect not seen with IRE alone. These results suggest that the systemic anti-tumor immune response triggered by IRE can be enhanced by stimulating the innate immune system with a TLR7 agonist and the adaptive immune system with anti-PD-1 checkpoint blockade simultaneously. Combinatorial approaches such as this may help overcome the immunosuppressive pancreatic cancer microenvironment.

### Keywords

Irreversible Electroporation; Pancreatic Cancer; Immunotherapy; Neoantigens; TLR7 stimulation

**Corresponding Author:** Rebekah Ruth White, M.D, FACS. UC San Diego Health - La Jolla, Moores Cancer Center, 3855 Health Sciences Drive, La Jolla, CA 92093. rewhite@ucsd.edu.

Conflict of Interest

Authors declare no conflict of interest.

## Introduction

Over 50,000 patients are diagnosed with pancreatic cancer each year in the US, and over 40,000 will die from it [1]. Most patients present with metastatic disease or develop distant metastatic disease despite treatment of localized disease. Palliative chemotherapy is the only approved treatment option for these patients, and response rates are low [2, 3]. Immune checkpoint inhibitors have demonstrated clinical responses in a number of solid malignancies, but results in pancreatic cancer have been disappointing [4, 5]. Pancreatic cancer has only a moderate mutational burden, the factor most correlated with response to immune checkpoint inhibitor therapy [6]. In addition, the pancreatic cancer microenvironment is immunosuppressive. Its desmoplastic stroma contains few effector T cells and a surfeit of immunosuppressive leukocytes, including tumor-associated macrophages, myeloid derived suppressor cells (MDSCs), and regulatory T cells (Tregs)[7].

Irreversible electroporation (IRE) has been developed as a non-thermal method of inducing tumor cell death without destroying adjacent collagenous structures [8]. This technology, marketed as Nanoknife® (Angiodynamics), has 510(k) clearance from the FDA and is being used clinically for selected patients with locally advanced PC [9–13]. The most common pattern of recurrence in these studies was distant progression, emphasizing the need for better methods to treat micrometastatic disease.

Ablative techniques may induce anti-tumor immune responses by increasing the availability of tumor specific antigens in an inflammatory context. Neoantigens released by the tumor are cross-presented by antigen presenting cells (APCs) to activate tumor-specific T cell responses. Several studies have demonstrated that thermal ablation induces systemic anti-tumor immune responses in multiple tumor types [14]. A limited number of studies have examined the immune effects of IRE. Li et al. showed that IRE results in multiple changes in peripheral cytokines and lymphocytes, including increased interferon(IFN)-γ-positive splenocytes, in a rat osteosarcoma model [15]. Neal et al. demonstrated that IRE generates systemic immune responses in murine subcutaneous ~~(SQ)~~ renal cell carcinoma models in which the growth of secondary, contralateral tumors was reduced by IRE of a primary tumor two weeks earlier [16]. In a study by Zhao et al. using an orthotopic murine pancreatic cancer model, IRE alone was shown to induce transient softening of the tumor stroma, increased microvascular density, and increased permeability [17]. They furthermore showed that IRE reversed resistance to anti-programmed death-1 receptor (PD-1) therapy, inducing $CD8^+$ T cell infiltration and immunogenic cell death more effectively than did the combination of irradiation and anti-PD-1 therapy. It has been theorized that the preservation of acellular collagenous structures, such as blood vessels, by IRE may promote immune cell infiltration to a greater extent than does thermal ablation, but IRE and thermal ablation have not been directly compared.

In our clinical experience, we find that the immune effects of IRE alone are not sufficient to eradicate all distant micrometastatic disease in patients [9–12, 18]. The objective of this study was to combine IRE with immunotherapeutic adjuvants to augment anti-tumor immune responses. Antibodies against PD-1 (e.g., nivolumab and pembrolizumab) are now widely used with FDA approval for several advanced malignancies. Toll-like receptors

(TLRs) are expressed on APCs and play a role in innate immune responses to inflammation. TLR agonists have the potential to work synergistically with checkpoint inhibitors, which act on adaptive immune cells. This concept was supported by our study in which the effects of systemic PD-1 checkpoint inhibition were enhanced by intratumoral (IT) injections of TLR7 and/or TLR9 agonists in a murine model of head and neck cancer [19]. The TLR9 agonist (SD-101, Dynavax) is being studied in several clinical trials, whereas the phospholipid-conjugated TLR7 agonist (1V270) has only been tested in preclinical models. However, the TLR7 agonist was as effective as the TLR9 agonist in this study and induced less systemic cytokine release than did the TLR9 agonist [20, 21]. We hypothesize that activating the innate immune system through the TLR pathway will augment the processing of neoantigens released during IRE and that checkpoint inhibition will augment neoantigen-specific adaptive immune responses.

Using an immunocompetent mouse model of pancreatic cancer, we have demonstrated that IRE alone can serve as an “in situ vaccine” and induce systemic immune responses that prevent secondary tumor growth. We also show that combination of IRE with innate immune activators and PD-1 checkpoint blockade can have abscopal effects on established, untreated secondary tumors (therapeutic immunity). The combinatorial approach described in this study may help with overcoming the immunosuppressive pancreatic cancer microenvironment and achieving therapeutic responses in patients.

## Materials and Methods

### Cell lines

The male KPC4580P cell line was established from a spontaneous tumor that developed in a male LSL-*Kras*$^{G12D/+}$; LSL-*Trp53*$^{R172H/+}$; *Pdx1*$^{Cre/+}$; LSL-*Rosa*26 $^{Luc/+}$ (KPC-luc) mouse (generously provided by J.J. Yeh, University of North Carolina, in 2015). The generation of this cell line and information regarding growth conditions have previously been described [22]. Cells were cultured in DMEM-F12 (Gibco) supplemented with 10% FBS, 2 mM L-glutamine, 100 U/mL penicillin and 100 μg/mL streptomycin (Gibco) under standard conditions. The cell line was negative for mycoplasma and several mouse pathogens by Comprehensive IMPACT II testing (IDEXX Bioresearch). A tumor from the tested stock was sequenced for authentication (see Data Availability). Cells were used within 3 passages of being thawed from frozen aliquots of the tested stock for every experiment but were not reauthenticated in the past year.

### Animals and reagents

All animal experiments were approved by the Institutional Animal Care and Use Committee (IACUC) of University of California, San Diego (UCSD). Wild type (WT) C57BL/6 were purchased from Jackson Laboratories. *Rag-1* knockout mice were obtained from Jackson Laboratories and bred by the UCSD Animal Care Program. The TLR7 agonist, 1V270, was synthesized by our laboratory [23]. Rat anti–mouse PD-1 (clone J43, BE0033–2), rat anti-mouse CD8 (Clone YTS169.4, BE0117) and rat anti-mouse CD4 (Clone GK1.5, BE0003) monoclonal antibodies were purchased from BioXcell.

### *In vivo* experiments

In all IRE experiments, subcutaneous pancreatic tumors were initiated by implanting $5\times10^5$ KPC4580P cells in the left flank of 6–8 week old male C57BL/6 or *Rag-1* knockout mice. Male WT mice were used for gender compatibility with the male KPC4580P cell line. IRE was performed when tumors reached 5–6 mm diameter (8–10 days after implantation) using an ECM 830 square wave pulse electroporator (Harvard apparatus) with a 2-needle probe, separated by 5 mm, to deliver a total of 150 pulses at 1500 V/cm as previously described [24]. Mice were anesthetized with 2% isoflurane in 3 L/min oxygen flow and injected subcutaneously with buprenorphine analgesic (0.1 mg/Kg). The skin above the subcutaneous tumor was punctured, and the tumor was bracketed using the 2-needle probe followed by delivery of the electric pulses using a safety foot pedal control. For comparison, surgical resection was performed by excising tumors with a margin of grossly normal tissue using the same anesthetic conditions as IRE. Tumor rechallenge was performed on mice that were tumor-free after IRE or surgical resection with subcutaneous injection of $5\times10^5$ KPC4580P cells on the contralateral (right) flank. Age-matched C57BL/6 male mice with a single tumor challenge were used as controls for all rechallenge experiments. TLR7 agonist (1V270) was administered as an IT injection of 100 μg/animal every two days starting the day of IRE for three doses. Systemic anti-PD-1 injections of 200 μg/animal were given intraperitoneally (IP) every 2 days starting the day prior to IRE. Vehicle and rat IgG controls were administered in respective control mice. Adoptive cell transfer was performed in *Rag-1* knockout mice with T cells isolated from the spleen and lymph nodes of IRE responsive or tumor bearing control mice. $8\times10^6$ lymphocytes were isolated using density gradient centrifugation on sterile Lympholyte (Cedar Lane) with greater than 90% viability and injected subcutaneously into recipient *Rag-1* knockout mice along with $5 \times 10^5$ tumor cells.

### Analysis of tumor-infiltrating immune cells

Mice bearing subcutaneous tumors were euthanized 7 days after IRE, and tumors were harvested and a portion dissociated using a mouse tumor dissociation kit according to manufacturer's recommendations (Miltenyi Biotec). The cells were then passed through a 70 μm strainer to make single cell suspensions, and viability was measured using ViCell cell counter (Beckman Coulter). Single cell suspensions containing $3\times10^6$ cells/sample were stained on ice for 30 min in 50 μL total volume of brilliant staining buffer (BD biosciences) using appropriate fluorescent antibody cocktails (Listed in Supplementary Table S1) after Fc blocking. The samples were washed once and resuspended in 200 μL of cold PBS containing 2% FBS and 1 mM EDTA for analysis using flow cytometry (BD FACS Celesta/BioRad ZE5). Ultracomp compensation beads (Thermo Fisher Scientific) stained with single antibody fluorochrome combinations were used as compensation controls, and the detector voltages were set to achieve best compensation for the spectral overlap of the fluorochromes before acquisition of the study samples. Mouse splenocytes stained with the complete cocktail were used as a positive control, and fluorescence minus one (FMO) stained samples were used as negative controls for each antibody in the cocktail. Cells were fixed and permeabilized using intracellular staining reagents using the manufacturer's instructions (Intracellular Fixation & Permeabilization Buffer Set, eBioscience) for the staining of FoxP3 and IFNγ. Flow cytometry data were then analyzed using Flow Logic software (Miltenyi Biotec) [25].

### Immune cell depletion study

Male C57BL/6 mice were injected IP with anti-mouse CD8 or CD4 antibody at 3 doses of 250 μg/injection on consecutive days prior to tumor implantation[26], and subcutaneous tumors were implanted on the 5$^{th}$ day. Successful depletion was confirmed by flow cytometry of inguinal lymph nodes (Supplementary Fig. S1). The depletion was maintained by administering the depleting antibody intraperitoneally once a week until the end of the study. IRE was performed on these mice as described above.

### Cytokine expression analysis

Tumors were excised at days 1, 7 and 14 after IRE. Tumor tissues were snap frozen and homogenized in gentle tissue lysis buffer (Thermo Scientific), and lysates were collected in the presence of protease and phosphatase inhibitors (Pierce Protease and Phosphatase Inhibitor Mini Tablets, Thermo Scientific). Proteome Profiler Mouse Cytokine Expression Array (R&D systems) was used to capture intratumoral cytokines according to manufacturer's instructions. An array intensity measurement layout was created using ImageJ, and the area of the positive control spots was defined and used to define the area of test spots. All signal spots falling outside the filter layout were considered as artefacts. Chemiluminescence imtensity of the duplicate spots on the membranes was calculated using ImageJ [27]. The relative fold changes in chemiluminescence against control tumors at the same timepoints were compared.

### Immunohistochemistry

A portion of tumors harvested on day 7 post procedure was fixed in formalin and embedded in paraffin for immunohistochemical analyses (IHC). For IHC staining, slides containing serial tissue sections of paraffin embedded tumor tissue blocks were deparaffinized with xylene for 3 changes of 5 min each, hydrated using ethanol gradient (100%, 90% and 75%) for 2 changes of 5 min each, and quenched with methanol/hydrogen peroxide for 30 min, followed by antigen retrieval with 10 mM citrate buffer (pH=6) for 14 min at 20% power in a microwave owen. The slides were allowed to cool for 15 min and washed extensively with distilled water and with PBS for 3 changes of 5 min each. Tissue sections were blocked with 2% horse serum at room temperature for 30 min and incubated with primary antibodies (Listed in Supplementary Table S2) in PBS with 2% horse serum at 4° C overnight in a humidified chamber. After washing with PBS for 3 changes of 5 min each, the sections were incubated with biotinylated secondary antibody for 30 min at room temperature followed by HRP conjugation with ABC elite universal kit (Vector Laboratories) according to the manufacturer's instructions. DAB (3,3'-diaminobenzidine) solution was used to develop the staining, and counterstained with hematoxylin. The sections were dehydrated using an increasing gradient of ethanol (75%, 90% and 100%) and then mounted with a coverslip using clear permanent mounting media. Hematoxylin and eosin staining were also performed for histological analysis. The slides were imaged using an Olympus SC100 microscope at 20× magnification.

### TCR repertoire analysis

$CD8^+$ T cells were isolated from the spleen and draining lymph nodes of IRE-responsive mice subjected to tumor rechallenge for 14 days or control tumor-bearing mice for 14 days using CD8 specific magnetic cell sorting kit (Miltenyi Biotec). RNA was extracted, and cDNA specific to TCR gene sequences was generated using the manufacturer's recommended protocol for the Takara SMARTer Mouse TCR a/b Profiling Kit by Medegenome, Inc, Foster City. Next generation TCR sequencing and analysis using MixCR pipeline (MiLabs) was performed at Medgenome Inc. The resulting clone count data were analyzed for TCR clonal expansion and diversity indices according to methods previously described [19]. Briefly, clones with under 5 counts were removed and clonal fraction was calculated for each remaining clone and used as input into heatmap and cumulative clonal fraction plots.

### Tumor neoantigen specificity analysis

Untreated KPC4580P subcutaneous tumors were excised from euthanized C57BL/6 mice 14 days after implantation followed by DNA and RNA extraction using DNeasy mini kit (Qiagen) and Purelink RNA mini kit (Thermo Scientific). Whole exome sequencing and mRNA sequencing were performed using miSeq platform (Illumina) to identify expressed non-synonymous genetic variants present in the tumor, cross-referenced against C57BL/6 genome (See Data Availability). Variants were prioritized according to their ability to be presented by MHC molecules using prediction algorithms. Peptides (20 amino acids in length) harboring these potential antigens at positions 6 and 15 were synthesized by A&A Labs and pooled into peptide pools of 10 each (List of KPC peptides, Supplementary Information). Bone marrow derived dendritic cells (BMDCs) were generated from male C57BL/6 mice as described earlier [28]. Briefly, tibia from an age matched male C57BL/6 mouse was excised asceptically, and the bone marrow was collected by rinsing with 10 mL of sterile PBS. Cells were resuspended at a concentration of $1 \times 10^6$ cells/mL in BMDC media (RPMI1640 10% FBS + 15 mM HEPES + 50 μM β-Mercaptoethanol) containing 20 ng/mL of IL-4 and GM-CSF, grown at standard conditions for 6 days. On day 6, the concentration of IL-4 and GM-CSF was increased to 40 ng/mL, and the BMDCs in suspension were collected on day 7. The BMDCs were incubated with 5 μg/mL of mutant peptides pools to facilitate antigen presentation for 1 day at 37° C. A pre-wet multiscreen-IP filter plate (Millipore) was coated with 50 μL/well of 2 μg/mL IFNγ capture antibodies (AN18; Mabtech) diluted in PBS at 4° C overnight. The plate was washed thrice with PBS and blocked with RPMI media containing 10% FBS for 1 h. $2 \times 10^5$ lymphocytes isolated from IRE-responsive mice were incubated with 5 μg/mL of the different mutant peptides pools in each well of the IFNγ capture filter plates for 30 min at 37° C, 5% $CO_2$. 5 μg/mL of concanavalin A (Sigma-Aldrich) was used as the positive stimulus control and no peptide wells were used as negative control. Then 20,000 activated BMDCs generated earlier were added to the wells containing the respective peptide pools with lymphocytes, and the co-culture was incubated for 20 h at 37° C 5% $CO_2$. Lymphocytes from naïve (non-tumor bearing) mice were used as negative controls along with lymphocytes from untreated tumor bearing (Tumor) mice and mice subcutaneously injected with irradiated $5 \times 10^6$ KPC4580P cells followed by live cell rechallenge (Vaccinated). The cells were discarded from the plate after incubation and washed 6 times with PBS + 0.05% Tween 20 and incubated with 100

μL/well of 1μg/mL biotinylated anti-mouse IFNγ (R4–6A2; Mabtech) in PBS + 0.5% BSA for 2 h at 37° C. Avidin peroxidase conjugation was performed using an APC kit (Vector Laboratories), and the plate was developed using 100 μL/well of 3-Amino-9-ethylcarbazole (Sigma-Aldrich) for 10 min. The plate was washed, dried, and imaged using an ELISPOT reader, and the wells with >100 SFC/$10^6$ cells more than the negative control were considered positive. Peptide pools that were positively recognized by T cells (expressed IFNγ) were then deconvoluted using the same procedure to identify the individual antigens recognized by T cells.

### Data availability

Sequencing data for mutational profiling, TCR sequencing, and RNA-sequencing are available under the NCBI BioProject link http://www.ncbi.nlm.nih.gov/bioproject/545738.

### Statistical methods

All results were expressed as means ± standard error of the mean (SEM). Statistical difference between groups was calculated either using the student *t* test or ANOVA with post-hoc multiple comparisons depending on the data, using GraphPad Prism 8.0 software. A value of $P < 0.05$ was considered significant.

## Results

To assess the efficacy of IRE as a monotherapy against pancreatic cancer, immunocompetent male C57BL/6 mice were treated with IRE when subcutaneous KPC4580P tumors reached 5 mm in diameter (Fig. 1A). The most effective IRE dose and the immunogenicity of this cell line in C57BL/6 mice were determined in preliminary tumor growth and vaccination experiments, respectively (Supplementary Fig. S1). Monotherapy with IRE significantly inhibited tumor growth compared to control mice (P<0.01, Fig. 1B). Survival was monitored until tumor diameter reached 15 mm and was significantly prolonged in the IRE group (Fig. 1C). IRE induced complete tumor regression in 3 of 9 mice at 14 days post treatment (Fig. 1D). Over repeated experiments, 20%–35% of mice had complete responses and did not demonstrate tumor recurrence after 6 months of monitoring.

To assess the role of the immune system in the efficacy of IRE, *Rag-1* knockout mice, which lack mature T and B lymphocytes, were subjected to the same IRE treatment on subcutaneous KPC4580P tumors. Tumors in both the treatment and control groups grew faster than tumors in immunocompetent mice, with no apparent difference between groups (Fig. 1E). This emphasizes the need for an active adaptive immune system for IRE to be effective. Depletion of different subsets of immune cells independently allowed us to identify $CD8^+$ and $CD4^+$ T-cells as players in eliciting the anti-tumor response following IRE (Fig. 1F, Supplementary Fig. S1). $CD8^+$ T cell depletion prevented anti-tumor response to IRE with a growth curve similar to the control group. $CD4^+$ T cell depleted mice did not respond to IRE, and tumors grew more rapidly than in the untreated immunocompetent mice, suggesting $CD4^+$ T helper cells are the most important. The innate immune components, NK cells and macrophages, also contribute to anti-tumor immunity, since their

depletion reduced IRE efficacy compared to IRE in an immunocompetent mouse (Supplementary Fig. S1).

Having shown that an intact immune system is necessary for IRE to be effective, we assessed the effects of IRE on the tumor microenvironment (Fig. 2). IRE-treated tumors displayed evidence of cell death consistent with the ablative effects of IRE (Fig. 2A). Immunohistochemical staining with anti-CD45 showed areas of increased immune cell infiltration into the tumor after IRE. Although there was no visible increase in the infiltrating $CD4^+$ T cell population by IHC (Fig. 2A), there was an apparent increase in the infiltration of $CD8^+$ T cells (Fig. 2A). By flow cytometry, there was greater variability in the immune profiles of IRE-treated than in control tumors (Fig. 2B), likely due to variability in response. Most of the differences between IRE-treated and control tumors, including CD45+ cells, $CD8^+$ T cells, effector $CD8^+$ T cells staining positively for intracellular IFNγ, and the ratio of pro-inflammatory M1-type macrophages ($CD11b^+F4/80^+MHCII^{hi}CD206^{lo}$) to M2-type macrophages ($CD11b^+F4/80^+MHCII^{lo}CD206^{hi}$) [29] did not achieve significance. The only significant difference was the immunosuppressive population of MDSCs that comprised 9.9% of total $CD45^+$ cells in the control group and was reduced to 3.2% after IRE ($P < 0.05$).

Cytokines in the tumor microenvironment recruit or prevent the infiltration of immune cells. We examined intratumoral cytokines at one week in mice without complete responses to IRE and detected increases in IFNγ, I-309 (CCL1), and IL-2, suggesting Th1 response (Fig. 2C). There was an immediate and sustained decrease in tumor-associated CXCL1, a driver for MDSC recruitment and $CD8^+$ T cell exclusion [30]. An increase in CXCL3, a monocyte chemoattractant induced by IFNγ was also observed. Th2 markers IL-4 and IL-6 were decreased after IRE, whereas an increase in IL-10, a Th2 wound healing response expected after ablation, was not statistically significant (Supplementary Fig. S2). We also examined plasma cytokines one week after IRE, comparing mice without complete response (non-responders) to mice with complete response (responders), who did not have tumors for analysis of intratumoral cytokines (Supplementary Fig. S3). We observed a trend towards an increase in IFNγ after IRE, with differential effects seen between complete responders and non-responders on IFNγ and CXCL1, but these differences did not achieve statistical significance due to the relatively small number of complete responders.

Since surgical resection is considered the optimal treatment for localized tumors, we compared the outcomes of mice harboring tumors treated with IRE versus radical resection (Fig. 3A). Surgical resection was more effective at controlling the primary tumor in this model with no evidence of tumor in 6 of 10 mice at 21 days as compared to 3 of 10 mice in the IRE group (Fig. 3B). This local recurrence rate after radical resection is a testament to the aggressive nature of these tumors. However, when tumor-free mice were rechallenged 14 days later with a subcutaneous injection of live KPC4580P cells on the contralateral flank, no tumors grew in the tumor-free mice from the IRE group. In contrast, secondary tumors grew in 3 of 5 tumor-free mice from the surgical resection group (Fig. 3C, D). Rechallenged IRE mice were monitored for 6 months and showed no evidence of recurrence. This demonstrates that successful ablation with IRE alone can induce prophylactic immunity, acting as an “in situ” vaccine against subsequent tumor rechallenge.

IRE's ability to induce protective immunity against future tumor rechallenge prompted us to study if IRE generates tumor antigen-specific T cell responses. RNA and DNA were isolated from KPC4580P subcutaneous tumors in order to identify tumor-specific (against WT C57BL/6 background) expressed non-synonymous variants using whole exome sequencing and RNA sequencing (RNAseq). Identified variants are depicted in a Circos plot (Supplementary Fig. S4), and 44 variants were prioritized based on their high RNA expression and sequencing depth. Most of the identified variants were single nucleotide polymorphisms resulting from the mixed background of the KPC4580P model. However, these model inherent alloantigens were specific to the tumor, relative to the C57BL/6 host, acting as surrogates for tumor neoantigens. Peptides representing potential antigens were tested for their ability to induce IFNγ secretion in T cells isolated from naïve, tumor bearing, vaccinated or IRE-treated and rechallenged mice. Representative ELISPOT results (Fig. 4A) show that both IRE and vaccinated T cells show reactivity against peptides from pool 2 and pool 6 peptides. IRE alone showed reactivity to pool 9 and pool 1 peptides, and vaccination group alone showed reactivity to pool 3. The reactivities were consistent only against pool 2, pool 6 and pool 9 across three independent experiments and were the only pools deconvoluted (Fig. 4B). Although pool 9 collectively induced IFNγ secretion, none of the individual peptides had a significant signal. From pool 2, *Car12* and *Cdk12* peptides were recognized by T cells from IRE mice but not by T cells from tumor bearing mice. The *Hook2* peptide in pool 6 was recognized by both IRE-treated and vaccinated mice, whereas *HPS1* was recognized only by the tumor-bearing and IRE-treated mice. The fact that 4 out of the 5 peptides with reactivity were recognized significantly by T cells from IRE-treated mice, versus only one in tumor-bearing mice, emphasizes that the presence of the antigen alone is not sufficient for the recognition of most antigens. It also suggests that IRE increased recognition of weaker antigens by the immune system. The recognition patterns of T cells from IRE-treated mice were similar to, if not better than, those from mice vaccinated with irradiated tumor cells, supporting the hypothesis that IRE induces an "in situ" vaccination effect.

To further investigate the systemic immune effects of the IRE model, T-cell receptor (TCR) sequencing was performed on the $CD8^+$ T cells isolated from tumor bearing control mice and IRE responsive mice. The differences in relative abundance of the individual T cell clones between representative individual mice are shown (Fig. 4C). None of the clones exceeded 0.2% of total TCR clonotypes in the control mouse, indicating a lack of active systemic CD8 T cell activation. In the IRE mouse, in contrast, several clones constituted more than 0.4% of the total clones with the top clone constituting 0.8%, suggesting an enrichment of specific $CD8^+$ T cell clones. Despite the lack of a significant difference in the diversity indices, clonal expansion within the top 100 clones was more apparent in the IRE mice compared to control mice (Fig. 4D). It cannot be concluded that the enriched clones are tumor specific. However, from the combination of increased tumor mutant antigen recognition (Fig. 4A, B) with elevated T cell clonal expansion (Fig. 4E) after IRE, it can be postulated that IRE can induce systemic T cell activation. Adoptive transfer of these systemic post-IRE T cells into *Rag-1* knockout mice, along with live KPC4580P cells SQ prevented growth of this allogeneic tumor in immunocompromised mice ($P<0.001$) without prior exposure (Fig. 4E). In contrast, T cells from tumor-bearing donor WT mice were not

able to prevent tumor growth in 4/5 recipient *Rag-1* knockout mice. These results show that tumor alone is not sufficient to induce an effective systemic adaptive immune response. IRE not only reduces tumor burden but also helps to protect from future recurrences by inducing T cell-mediated protective immunity.

To test the ability of IRE to induce a systemic immune response against a concomitant distant untreated tumor, C57BL/6 mice were injected with KPC4580P cells SQ in both flanks simultaneously. The larger of the two tumors was treated with IRE 7 days after implantation. IRE failed to elicit anti-tumor responses against either the primary or contralateral tumor, in contrast to the robust anti-tumor responses observed when only a single tumor was present (Supplementary Fig. S5A, B). The loss of efficacy in the setting of increased secondary tumor burden demonstrates the sensitivity of IRE to immunosuppression and emphasizes the need to improve immune responses using combination immunotherapeutic strategies.

Consistent with clinical studies in humans [5, 31], checkpoint inhibition alone was not effective against subcutaneous KPC tumors (Fig. 5A). The combination of anti-PD-1 and IRE was significantly more effective than anti-PD-1 alone but not better than IRE alone in improving tumor growth or overall survival (Fig. 5B). Complete responders to either IRE or the combination of IRE and PD-1 were protected from subsequent tumor rechallenge (Fig. 5C). Tumor analysis by flow cytometry did not reveal significant inceases in $CD8^+$ T cell infiltration (Fig. 5D) or M1/M2 macrophage ratio (Fig. 5E), but there was a significant reduction in MDSCs with IRE and anti-PD-1 therapy (Fig. 5F).

The other strategy we tested was to target the innate immune system using TLR7 agonist 1V270. Similar to anti-PD-1 therapy, IT 1V270 injections showed no additive improvement over IRE alone in tumor growth reduction, survival or protection against rechallenge (Fig 5 G,H and I). Although ineffective against KPC tumors as a monotherapy (Supplementary Fig. S5C), IT injections of 1V270 with IRE significantly improved the M1/M2 ratio (Fig. 5J) without improvements in $CD8^+$ T cell infiltrates or MDSCs over IRE alone (Fig. 5K, L). These results suggested that the incremental improvements offered by either anti-PD-1 or 1V270 alone are not sufficient to overcome the aggressive nature of these tumors, but perhaps can be combined to achieve a more robust immune response.

A second study was performed in which the secondary tumor was implanted 7 days after the primary tumor on the contralateral flank, then the primary tumor was treated 3 days later, modeling micrometastatic spread from a primary tumor. Under these conditions, primary tumor growth was significantly reduced after IRE ($P<0.05$) and the combination of IRE + 1V270 + anti-PD-1 ($P<0.001$, Fig. 6A, B). After IRE alone, the untreated secondary tumors grew more slowly after IRE than in the control mice (Fig. 6C, D), but only one tumor completely regressed. However, the combination of IRE + 1V270 + anti-PD-1 was more effective at preventing growth of tumors on the untreated site, with 5 of 9 mice demonstrating complete regression ($P< 0.001$, Fig. 6D).

Finally, we examined the immune profiles of distant tumors from the previous abscopal experiment. By IHC (Fig. 7A), immune cell infiltration could be seen approaching from the

periphery towards the center in the combination group. $CD8^+$ cytotoxic T cell staining was elevated in tumors treated with the combination compared to control tumors or tumors treated with IRE alone. By flow cytometry, the greater than 4-fold increase in IFNγ-secreting $CD8^+$ T cells compared to IRE alone further demonstrates the efficacy of this combination (Fig. 7B). Whereas we observed a decrease in the MDSC population in primary tumors treated with IRE (Fig. 2B), a difference in MDSCs was not observed in distant tumors responding to abscopal effects of IRE. The combination had an effect on other myeloid populations, as it increased the M1/M2 ratio without having any effect on total tumor associated macrophages. Finally, the increase in $CD8^+$ DCs, which mediate tumor antigen cross presentation to the $CD8^+$ T cells, supports the hypothesis that combination therapy of IRE with 1V270 and anti-PD-1 enhances antigen presentation.

## Discussion

IRE is an ablative therapy that is being used in selected patients with locally advanced pancreatic cancer who are not candidates for resection. Although experienced centers have reported local control rates greater than 90%, most patients develop distant recurrence [9–12]. Using an immunocompetent pancreatic cancer mouse model, we have demonstrated that IRE requires an intact immune system for efficacy and that IRE is capable of inducing systemic adaptive immune responses and prophylactic immunity to tumor rechallenge. This study extends work on IRE by Neal et.al., which showed that IRE is more effective in immunocompetent than in nude mice and that IRE induces robust local $CD3^+$ T cell infiltration [16]. In our study, surgical resection was superior to IRE in achieving local tumor control, but surgical resection did not effectively induce prophylactic immunity, demonstrating that the mere presence of tumor is not sufficient to induce adaptive immune responses. IRE can act as an “in situ vaccine”, generating neoantigen-specific T cell responses that confer protection against tumor growth by adoptive cell transfer into treatment-naïve immunocompromised mice. We have established the role of the adaptive immune system, particularly T-cells, in IRE mediated anti-tumor activity.

The study by Zhao et al. modeled incomplete IRE ablation [17], with approximately 7 mm orthotopic pancreatic tumors treated with the same 2-needle probes, separated by 5 mm, used in our study for 5–6 mm subcutaneous tumors. They observed no significant therapeutic effect on local tumor growth after IRE alone and no complete responses. However, even incomplete IRE helped to overcome resistance to checkpoint blockade with a prolongation of survival. In our study, IRE alone had effects on local tumor growth. The addition of anti-PD-1 antibody or local innate immune stimulation with a TLR7 agonist had at least additive effects on local tumor immune infiltrates but no effects on local tumor growth over IRE alone. The combination of IRE with checkpoint inhibition and TLR7 agonist, however, not only improved the local effects of IRE but also generated therapeutic abscopal effects against small secondary tumors, modeling the potential eradication of distant micrometastatic disease.

Our study has several limitations. First, complete responses were achieved in only 20–35% of mice with IRE alone. This is likely attributable to the technical difficulty of achieving complete ablation in small tumors using fixed two-needle probes. In humans, probes can be

positioned individually to precisely bracket the tumor, and change in resistance can be monitored in real time to confirm successful ablation [32]. Our model, however, arguably simulates the common situation in human patients in which occult local invasion results in incomplete ablation. Second, the abscopal effects observed with the combination of IRE with anti-PD1 and TLR7 agonist therapy were modest and only evident when the secondary tumor was smaller than the primary tumor. This models the clinical scenario in which IRE is typically performed, with a locally advanced primary tumor with micrometastatic disease, but we anticipate achieving better responses with optimized combinations of immune adjuvants. Third, most of the genetic variants identified in this tumor model were single nucleotide polymorphisms resulting from inadequate backcrossing of the genetically engineered mouse model from which the cell line was generated [22]. Mutations in homologous human proteins are therefore unlikely to be identified as neoantigens in human patients with pancreatic cancer. Although most of these genetic variants did not arise from somatic mutations within the tumor, the mutational burden in this cell line is comparable to the mutational burden seen in most human pancreatic cancers. The identified model inherent alloantigens may be useful to other researchers using KPC cell lines, and the demonstrated reactivity to these antigens demonstrates proof-of-concept. Finally, subcutaneous models do not fully recapitulate the pancreatic microenvironment. Ongoing studies will examine IRE and combination immunotherapy in orthotopic models that better represent the dense stroma and complex microenvironment of human tumors.

A phase II clinical trial is assessing the safety and efficacy of IRE with postoperative nivolumab in patients with locally advanced pancreatic cancer at the University of Louisville (). Local delivery of 1V270 or other innate immune stimulators at the time of IRE (and/or perioperatively by endoscopic ultrasound-guided injection) would be feasible and also warrants clinical investigation as a way to decrease both local and distant recurrence. “Abscopal” effects were originally described in reference to distant effects of tumor irradiation. Numerous preclinical studies have demonstrated synergistic effects of radiation with immunotherapy in other tumor types, but only a few have focused on pancreatic cancer, which is relatively radioresistant [33–36]. The role of chemoradiation in pancreatic cancer has been threatened by negative phase III clinical trials [37, 38], but multiple early phase clinical trials are evaluating the combination of irradiation with various immunotherapeutic strategies [39]. Zhao et al. found the combination of IRE and checkpoint inhibition to be more effective than the combination of irradiation and checkpoint inhibition in their model [17]. However, similar to IRE, the advanced radiation techniques in use today (such as stereotactic body radiation therapy) are difficult to model in mice [40], and direct comparison in humans will be necessary. Ultimately, a clinical strategy combining local ablation with agents that enhance both the adaptive and innate immune systems will likely be necessary to prevent recurrence in this recalcitrant disease.

## Supplementary Material

Refer to Web version on PubMed Central for supplementary material.

## Acknowledgments

Funding Support

This work was supported by the Padres Pedal the Cause (#PTC2017). Bioinformatic analyses were partially supported by a voucher from the Altman Clinical and Translational Research Institute at UCSD, which is funded by the National Institutes of Health (CTSAUL1TR001442). Immunohistochemistry was performed by the UCSD Moores Cancer Center Biorepository and Tissue Technology Shared Resource, which is funded by the National Cancer Institute (NCI P30CA23100). The content is solely the responsibility of the authors and does not necessarily represent the official views of the NIH.

## References

1. Siegel RL, Miller KD, and Jemal A, Cancer statistics, 2018. CA Cancer J Clin, 2018 68(1): p. 7–30. [PubMed: 29313949]
2. Conroy T, Desseigne F, Ychou M, Bouche O, Guimbaud R, Becouarn Y, et al., FOLFIRINOX versus gemcitabine for metastatic pancreatic cancer. N Engl J Med, 2011 364(19): p. 1817–25. [PubMed: 21561347]
3. Von Hoff DD, Ervin T, Arena FP, Chiorean EG, Infante J, Moore M, et al., Increased survival in pancreatic cancer with nab-paclitaxel plus gemcitabine. N Engl J Med, 2013 369(18): p. 1691–703. [PubMed: 24131140]
4. Brahmer JR, Tykodi SS, Chow LQ, Hwu WJ, Topalian SL, Hwu P, et al., Safety and activity of anti-PD-L1 antibody in patients with advanced cancer. N Engl J Med, 2012 366(26): p. 2455–65. [PubMed: 22658128]
5. Royal RE, Levy C, Turner K, Mathur A, Hughes M, Kammula US, et al., Phase 2 trial of single agent Ipilimumab (anti-CTLA-4) for locally advanced or metastatic pancreatic adenocarcinoma. J Immunother, 2010 33(8): p. 828–33. [PubMed: 20842054]
6. Schumacher TN and Schreiber RD, Neoantigens in cancer immunotherapy. Science, 2015 348(6230): p. 69–74. [PubMed: 25838375]
7. Clark CE, Hingorani SR, Mick R, Combs C, Tuveson DA, and Vonderheide RH, Dynamics of the immune reaction to pancreatic cancer from inception to invasion. Cancer Res, 2007 67(19): p. 9518–27. [PubMed: 17909062]
8. Davalos RV, Mir IL, and Rubinsky B, Tissue ablation with irreversible electroporation. Ann Biomed Eng, 2005 33(2): p. 223–31. [PubMed: 15771276]
9. Martin RC 2nd, Kwon D, Chalikonda S, Sellers M, Kotz E, Scoggins C, et al., Treatment of 200 locally advanced (stage III) pancreatic adenocarcinoma patients with irreversible electroporation: safety and efficacy. Ann Surg, 2015 262(3): p. 486–94; discussion 492–4. [PubMed: 26258317]
10. Kluger MD, Rashid MF, Rosario VL, Schrope BA, Steinman JA, Hecht EM, et al., Resection of Locally Advanced Pancreatic Cancer without Regression of Arterial Encasement After Modern-Era Neoadjuvant Therapy. J Gastrointest Surg, 2018 22(2): p. 235–241. [PubMed: 28895032]
11. Huang KW, Yang PC, Pua U, Kim MD, Li SP, Qiu YD, et al., The efficacy of combination of induction chemotherapy and irreversible electroporation ablation for patients with locally advanced pancreatic adenocarcinoma. J Surg Oncol, 2018 118(1): p. 31–36. [PubMed: 29878378]
12. Narayanan G, Hosein PJ, Beulaygue IC, Froud T, Scheffer HJ, Venkat SR, et al., Percutaneous Image-Guided Irreversible Electroporation for the Treatment of Unresectable, Locally Advanced Pancreatic Adenocarcinoma. J Vasc Interv Radiol, 2017 28(3): p. 342–348. [PubMed: 27993507]
13. Holland MM, Bhutiani N, Kruse EJ, Weiss MJ, Christein JD, White RR, et al., A prospective, multi-institution assessment of irreversible electroporation for treatment of locally advanced pancreatic adenocarcinoma: initial outcomes from the AHPBA pancreatic registry. HPB (Oxford), 2019.
14. Chu KF and Dupuy DE, Thermal ablation of tumours: biological mechanisms and advances in therapy. Nat Rev Cancer, 2014 14(3): p. 199–208. [PubMed: 24561446]
15. Li X, Xu K, Li W, Qiu X, Ma B, Fan Q, et al., Immunologic response to tumor ablation with irreversible electroporation. PLoS One, 2012 7(11): p. e48749. [PubMed: 23139816]

16. Neal RE 2nd, Rossmeisl JH Jr., Robertson JL, Arena CB, Davis EM, Singh RN, et al., Improved local and systemic anti-tumor efficacy for irreversible electroporation in immunocompetent versus immunodeficient mice. PLoS One, 2013 8(5): p. e64559. [PubMed: 23717630]
17. Zhao J, Wen X, Tian L, Li T, Xu C, Wen X, et al., Irreversible electroporation reverses resistance to immune checkpoint blockade in pancreatic cancer. Nat Commun, 2019 10(1): p. 899. [PubMed: 30796212]
18. Holland MM, Bhutiani N, Kruse EJ, Weiss MJ, Christein JD, White RR, et al., A Prospective, Multi-institution Assessment of Irreversible Electroporation for Treatment of Locally Advanced Pancreatic Adenocarcinoma: Initial Outcomes from the AHPBA Pancreatic Registry. HPB (Oxford), 2019: p. in press.
19. Sato-Kaneko F, Yao S, Ahmadi A, Zhang SS, Hosoya T, Kaneda MM, et al., Combination immunotherapy with TLR agonists and checkpoint inhibitors suppresses head and neck cancer. JCI Insight, 2017 2(18).
20. Goff PH, Hayashi T, He W, Yao S, Cottam HB, Tan GS, et al., Synthetic Toll-Like Receptor 4 (TLR4) and TLR7 Ligands Work Additively via MyD88 To Induce Protective Antiviral Immunity in Mice. J Virol, 2017 91(19).
21. Goff PH, Hayashi T, Martinez-Gil L, Corr M, Crain B, Yao S, et al., Synthetic Toll-like receptor 4 (TLR4) and TLR7 ligands as influenza virus vaccine adjuvants induce rapid, sustained, and broadly protective responses. J Virol, 2015 89(6): p. 3221–35. [PubMed: 25568203]
22. Naqvi I, Gunaratne R, McDade JE, Moreno A, Rempel RE, Rouse DC, et al., Polymer-Mediated Inhibition of Pro-invasive Nucleic Acid DAMPs and Microvesicles Limits Pancreatic Cancer Metastasis. Mol Ther, 2018 26(4): p. 1020–1031. [PubMed: 29550075]
23. Chan M, Hayashi T, Kuy CS, Gray CS, Wu CC, Corr M, et al., Synthesis and immunological characterization of toll-like receptor 7 agonistic conjugates. Bioconjug Chem, 2009 20(6): p. 1194–200. [PubMed: 19445505]
24. Shankara Narayanan JS, Ray P, Naqvi I, and White R, A Syngeneic Pancreatic Cancer Mouse Model to Study the Effects of Irreversible Electroporation. J Vis Exp, 2018(136).
25. Efremova M, Rieder D, Klepsch V, Charoentong P, Finotello F, Hackl H, et al., Targeting immune checkpoints potentiates immunoediting and changes the dynamics of tumor evolution. Nature Communications, 2018 9(1): p. 32.
26. Gorbachev AV, Heeger PS, and Fairchild RL, CD4+and CD8+; T Cell Priming for Contact Hypersensitivity Occurs Independently of CD40-CD154 Interactions. The Journal of Immunology, 2001 166(4): p. 2323. [PubMed: 11160289]
27. Roy A, Femel J, Huijbers EJM, Spillmann D, Larsson E, Ringvall M, et al., Targeting Serglycin Prevents Metastasis in Murine Mammary Carcinoma. PloS one, 2016 11(5): p. e0156151–e0156151. [PubMed: 27223472]
28. Matheu MP, Sen D, Cahalan MD, and Parker I, Generation of bone marrow derived murine dendritic cells for use in 2-photon imaging. J Vis Exp, 2008(17).
29. Jiang H, Hegde S, Knolhoff BL, Zhu Y, Herndon JM, Meyer MA, et al., Targeting focal adhesion kinase renders pancreatic cancers responsive to checkpoint immunotherapy. Nat Med, 2016 22(8): p. 851–60. [PubMed: 27376576]
30. Li J, Byrne KT, Yan F, Yamazoe T, Chen Z, Baslan T, et al., Tumor Cell-Intrinsic Factors Underlie Heterogeneity of Immune Cell Infiltration and Response to Immunotherapy. Immunity, 2018 49(1): p. 178–193 e7. [PubMed: 29958801]
31. Patnaik A, Kang SP, Rasco D, Papadopoulos KP, Elassaiss-Schaap J, Beeram M, et al., Phase I Study of Pembrolizumab (MK-3475; Anti-PD-1 Monoclonal Antibody) in Patients with Advanced Solid Tumors. Clin Cancer Res, 2015 21(19): p. 4286–93. [PubMed: 25977344]
32. Dunki-Jacobs EM, Philips P, and Martin RC 2nd, Evaluation of resistance as a measure of successful tumor ablation during irreversible electroporation of the pancreas. J Am Coll Surg, 2014 218(2): p. 179–87. [PubMed: 24315888]
33. Twyman-Saint Victor C, Rech AJ, Maity A, Rengan R, Pauken KE, Stelekati E, et al., Radiation and dual checkpoint blockade activate non-redundant immune mechanisms in cancer. Nature, 2015 520(7547): p. 373–7. [PubMed: 25754329]

34. Azad A, Yin Lim S, D'Costa Z, Jones K, Diana A, Sansom OJ, et al., PD-L1 blockade enhances response of pancreatic ductal adenocarcinoma to radiotherapy. EMBO Mol Med, 2017 9(2): p. 167–180. [PubMed: 27932443]

35. Yasmin-Karim S, Bruck PT, Moreau M, Kunjachan S, Chen GZ, Kumar R, et al., Radiation and Local Anti-CD40 Generate an Effective in situ Vaccine in Preclinical Models of Pancreatic Cancer. Front Immunol, 2018 9: p. 2030. [PubMed: 30245691]

36. Rech AJ, Dada H, Kotzin JJ, Henao-Mejia J, Minn AJ, Twyman-Saint Victor C, et al., Radiotherapy and CD40 Activation Separately Augment Immunity to Checkpoint Blockade in Cancer. Cancer Res, 2018 78(15): p. 4282–4291. [PubMed: 29844122]

37. Hammel P, Huguet F, van Laethem JL, Goldstein D, Glimelius B, Artru P, et al., Effect of Chemoradiotherapy vs Chemotherapy on Survival in Patients With Locally Advanced Pancreatic Cancer Controlled After 4 Months of Gemcitabine With or Without Erlotinib: The LAP07 Randomized Clinical Trial. JAMA, 2016 315(17): p. 1844–53. [PubMed: 27139057]

38. Neoptolemos JP, Stocken DD, Friess H, Bassi C, Dunn JA, Hickey H, et al., A randomized trial of chemoradiotherapy and chemotherapy after resection of pancreatic cancer. N Engl J Med, 2004 350(12): p. 1200–10. [PubMed: 15028824]

39. Gajiwala S, Torgeson A, Garrido-Laguna I, Kinsey C, and Lloyd S, Combination immunotherapy and radiation therapy strategies for pancreatic cancer-targeting multiple steps in the cancer immunity cycle. J Gastrointest Oncol, 2018 9(6): p. 1014–1026. [PubMed: 30603120]

40. Koontz BF, Verhaegen F, and De Ruysscher D, Tumour and normal tissue radiobiology in mouse models: how close are mice to mini-humans? Br J Radiol, 2017 90(1069): p. 20160441. [PubMed: 27612010]

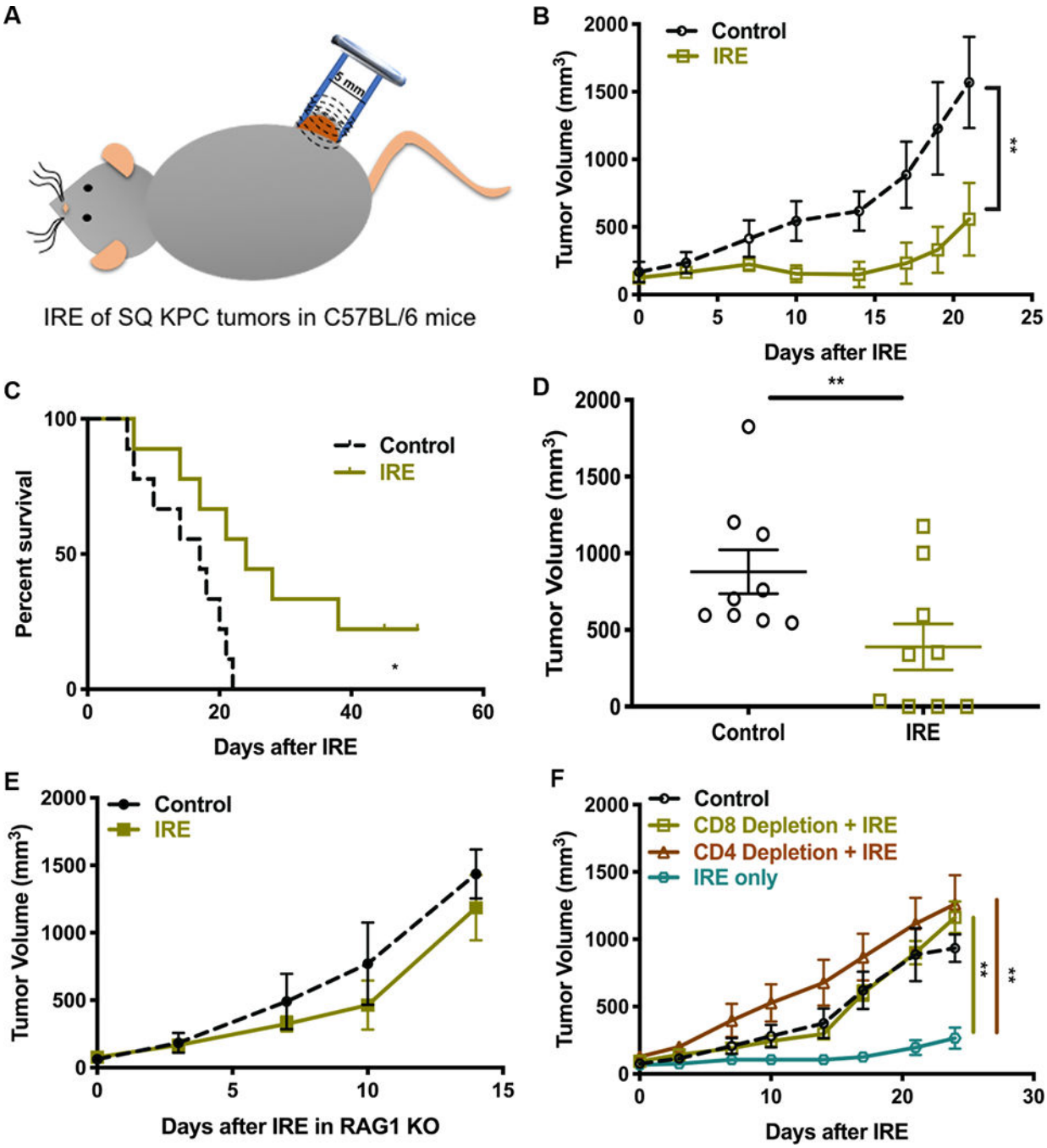


**Figure 1: Irreversible electroporation (IRE) of subcutaneous pancreatic tumors was effective only in the presence of an intact immune system.**

**(A)** Pictorial representation of the IRE procedure in subcutaneous KPC4580P tumors in C57BL/6 mice. Representative data from three independent experiments shown for **(B)** Growth curves of subcutaneous KPC4580P tumors, implanted 8 days before IRE, with and without IRE of the tumor (n=9/group). **(C)** Kaplan-Meier survival analysis post IRE. *P<0.05 by log-rank test. **(D)** Tumor size measurements of individual mice represented as dots with mean ± SEM on day 14. **P < 0.01 by 2-tailed Student's t-test. **(E)** Growth curves

of KPC4580P tumors in immunocompromised Rag-1 knockout mice with and without IRE treatment (n=6/group). **(F)** Representative data shown from two independent experiments of Immune cell depletion study showing growth curves of KPC4580P tumors in WT C57BL/6 mice depleted of either $CD4^+$ T cells $CD8^+$ T cells, or without such depletion and subjected to IRE (n=5/group). **P < 0.01 by two-way ANOVA with post hoc Tukey test.

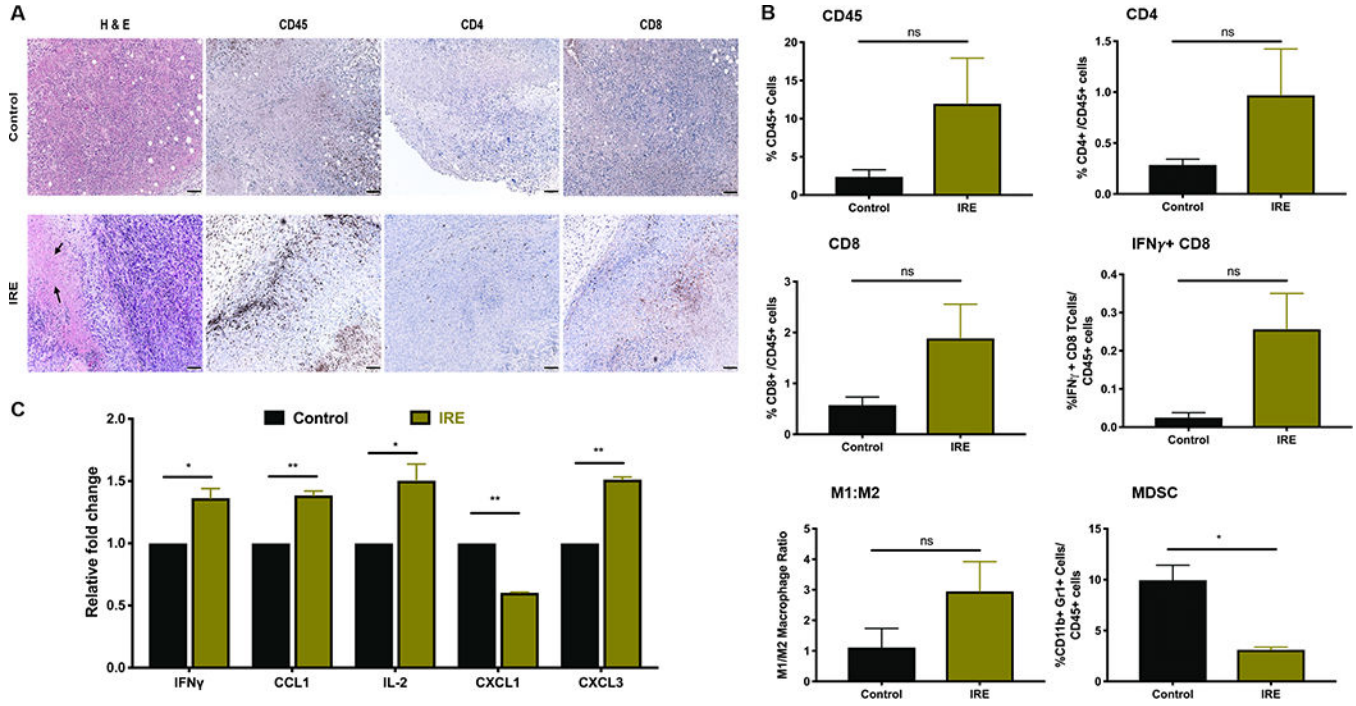


**Figure 2: IRE modulates the tumor immune microenvironment.**

**(A)** Representative image of three independent tissue stainings for H & E and IHC for CD45, CD4, and CD8 (blue – nucleus, brown – antigen) of untreated control and IRE-treated tumors harvested on day 7. Arrows indicate areas of cell death. All images taken at 20× magnification; scale bars represent 50 μm. **(B)** Flow cytometry analysis of immune infiltrates performed on day 7 on the harvested tumors (n=3/group). Enhanced immune infiltration and a proinflammatory microenvironment post combination therapy is evident from increased $CD8^+$, IFNγ+ $CD8^+$ (effector CD8), and M1:M2 ratio, and decreased MDSCs. Gating strategy is described in Supplementary Fig. S6. The data are representative of two independent experiments. **(C)** Intratumoral cytokine expression quantified using cytokine protein array from tumor samples excised at day 7. Chemiluminescence intensity values obtained for each time point for normalized to the untreated control value at the same time and expressed as relative fold change. * $P<0.05$, ** $P<0.01$ by 2-tailed Student's t-test. ns – not significant

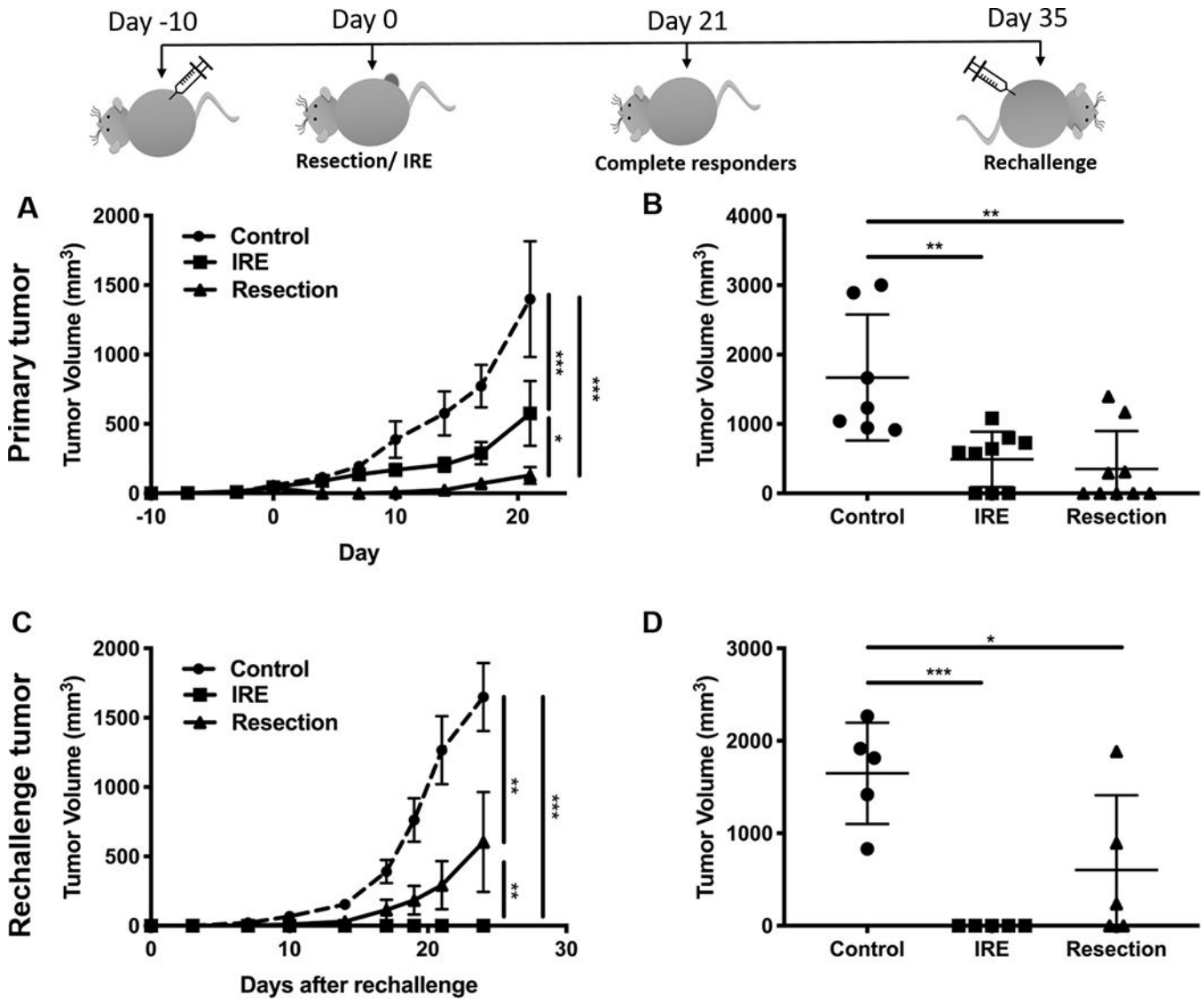


**Figure 3: IRE alone induces protective immunity in complete responders.**

Immunocompetent C57BL/6 mice with subcutaneous KPC4580P tumors were subjected to IRE or surgical resection of the primary tumor on Day 0, and mice with complete response to resection or IRE were rechallenged with KPC4580P tumor cells to the contralateral flank on day 35. Representative plots from 3 independent experiments of **(A)** primary tumor volumes represented as means ± SEM (n=10/group) and **(B**) tumor size measurements of individual mice represented as dot plots on day 21. **(C)** Secondary/rechallenge tumor growth rate on the contralateral flank on the complete responders (n=5/group), combined from two independent experiments, measured from day of rechallenge, compared to tumor challenge on age-matched, naive control mice. **(D)** Rechallenge tumor size measurements of individuals represented as dot plots on day 24 after rechallenge. *P < 0.05, **P < 0.01, ***P < 0.001 by two-way ANOVA with post hoc Tukey test (**A and C**) or by one-way ANOVA with post-hoc Bonferroni test (**B and D**).

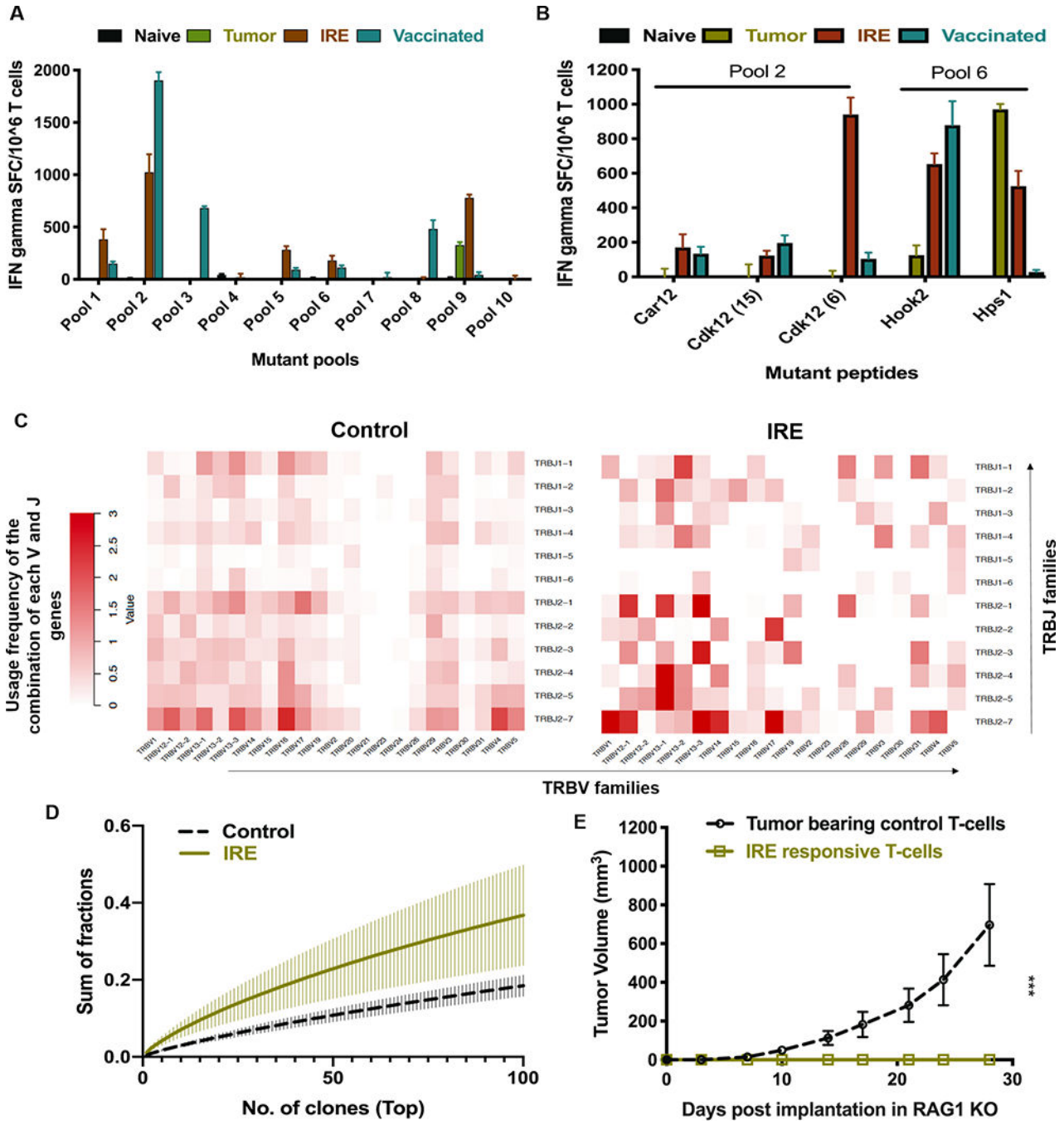


**Figure 4. IRE induces T-cell responses to model inherent antigens and increases TCR clonality expansion in tumor-bearing mice.**

**(A)** Representative IFNγ ELISPOT from peptide pools or **(B)** deconvoluted individual peptides using T cells isolated from groups of naïve mice (no tumor exposure), tumor-bearing mice, IRE-responsive mice (complete response to IRE) rechallenged with live tumor cells, and vaccinated mice (exposed to irradiated tumor cells then rechallenged with live tumor cells). Data represent mean ± SEM values of spot forming cells/10^6 cells from 3 independent mice per group in triplicates. Representative graph of three independent

experiments. **(C)** Representative heatmap of TCR repertoire clonalities of $CD8^+$ T cells. The x and y axes show the combination of V and J genes (TRBV and TRBJ families), and the z axis shows their frequency of usage. **(D)** Cumulative clonal fraction occupied by the top 1 – 100 $CD8^+$ T cell clones identified using TCR sequencing showing clonal expansion after IRE. **(E)** Adoptive transfer: KPC4580P tumor cells were injected subcutaneously in immunocompromised Rag-1 knockout mice along with $6 \times 10^6$ T cells from the spleen and lymph nodes of either tumor-bearing or IRE-responsive mice (n=5/group) represented as mean ± SEM. ***$P < 0.001$ by two-way ANOVA with post hoc Tukey test.

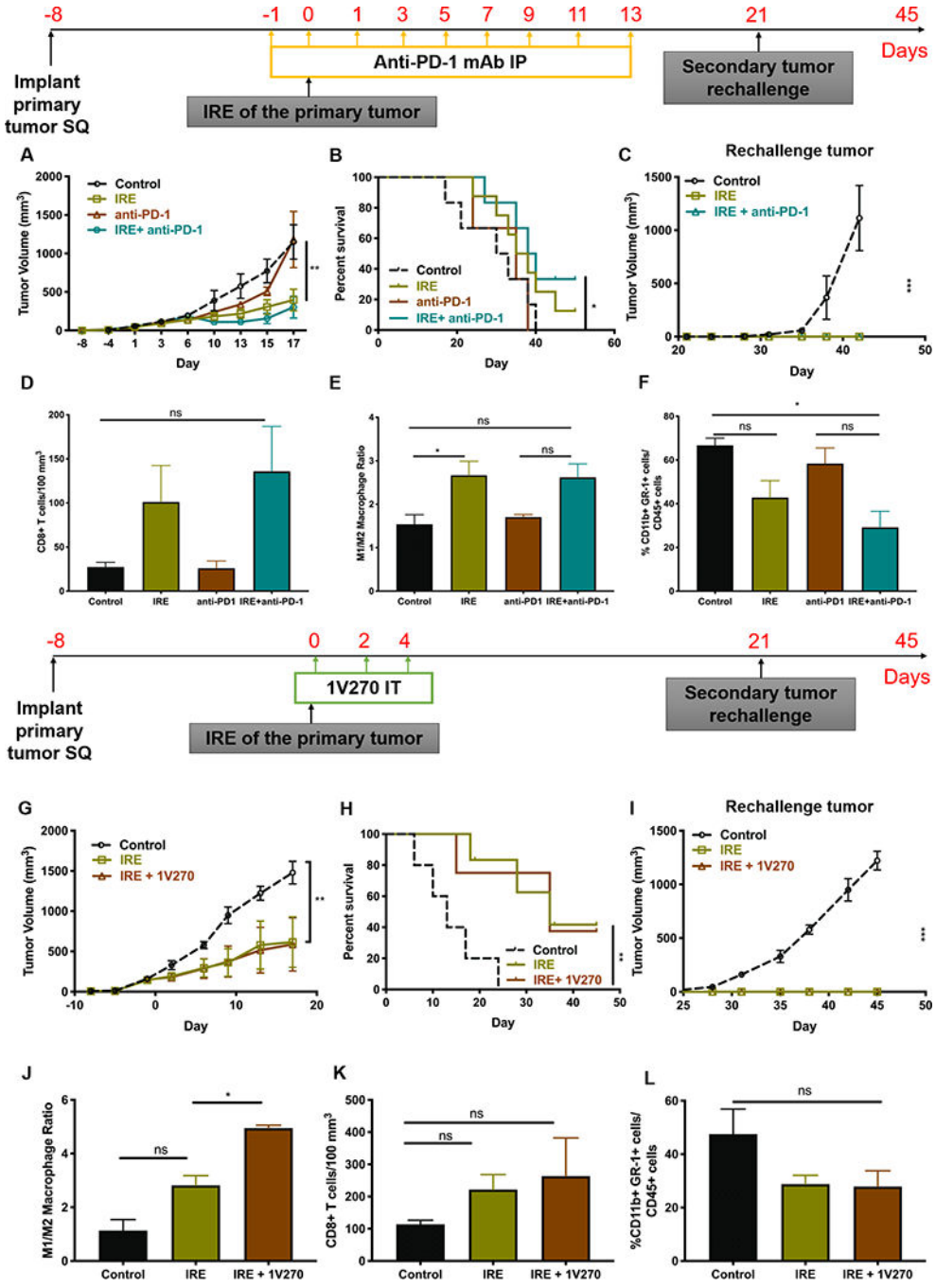


**Figure 5. The effects of IRE on the tumor microenvironment are improved by combination with immunotherapeutic agents.**

The timeline for treatment in each combination study is shown above the top panel (anti-PD-1, **A-F**) and bottom panel (TLR7 agonist 1V270, **G-L**). KPC4580P cells were implanted subcutaneously in WT C57BL/6 mice 8 days prior to IRE. Anti-PD-1 was given IP every 2 days starting day −1 to day 13 and 1V270 was given IT on days 0, 2 and 4. **(A and G)** Neither anti-PD-1 nor 1V270 had a significant additive effect over IRE on local tumor growth when combined with IRE (n=9/group). **P < 0.01, ***P < 0.001 by two-way

ANOVA with post hoc Tukey test. **(B and H)** Kaplan-Meyer survival analysis for same experiments with log-rank test *P < 0.05, **P < 0.01. **(C and I)** Similar to Fig. 3C above, mice with complete response to IRE with or with combination immunotherapy were protected from tumor rechallenge on the contralateral flank (n=4/group) **P < 0.01, ***P < 0.001 by two-way ANOVA with post hoc Tukey test. **(D and K)** Tumors were harvested and dissociated on day 7 (one week post IRE) for flow cytometric analysis of tumor-infiltrating immune cells. Tumor infiltrating $CD8^+$ T cells were gated out of live $CD45^+$ and $CD3^+$ cells. **(E and J)** Macrophage subpopulations were first identified as $CD45^+$ $CD11b^+$ $F4/80^+$ subsets under which $CD206^{lo}$ MHC-$II^{hi}$ were classified as M1 macrophages and $CD206^{hi}$, MHC-$II^{lo}$ were classified as M2 macrophages. From these, M1/M2 ratios were calculated and plotted. **(F and L)** Myeloid derived suppressor cells (MDSCs) were identified in dissociated tumors as $CD45^+$ $CD11b^+$ and Gr-$1^+$ subsets and their relative abundance in terms of the total immune cells is plotted. Flow cytometry plots are representative plots of two independent experiments represented as means ± SEM (n=3/group) *P < 0.05, ns – not significant by one-way ANOVA with post hoc Bonferroni test.

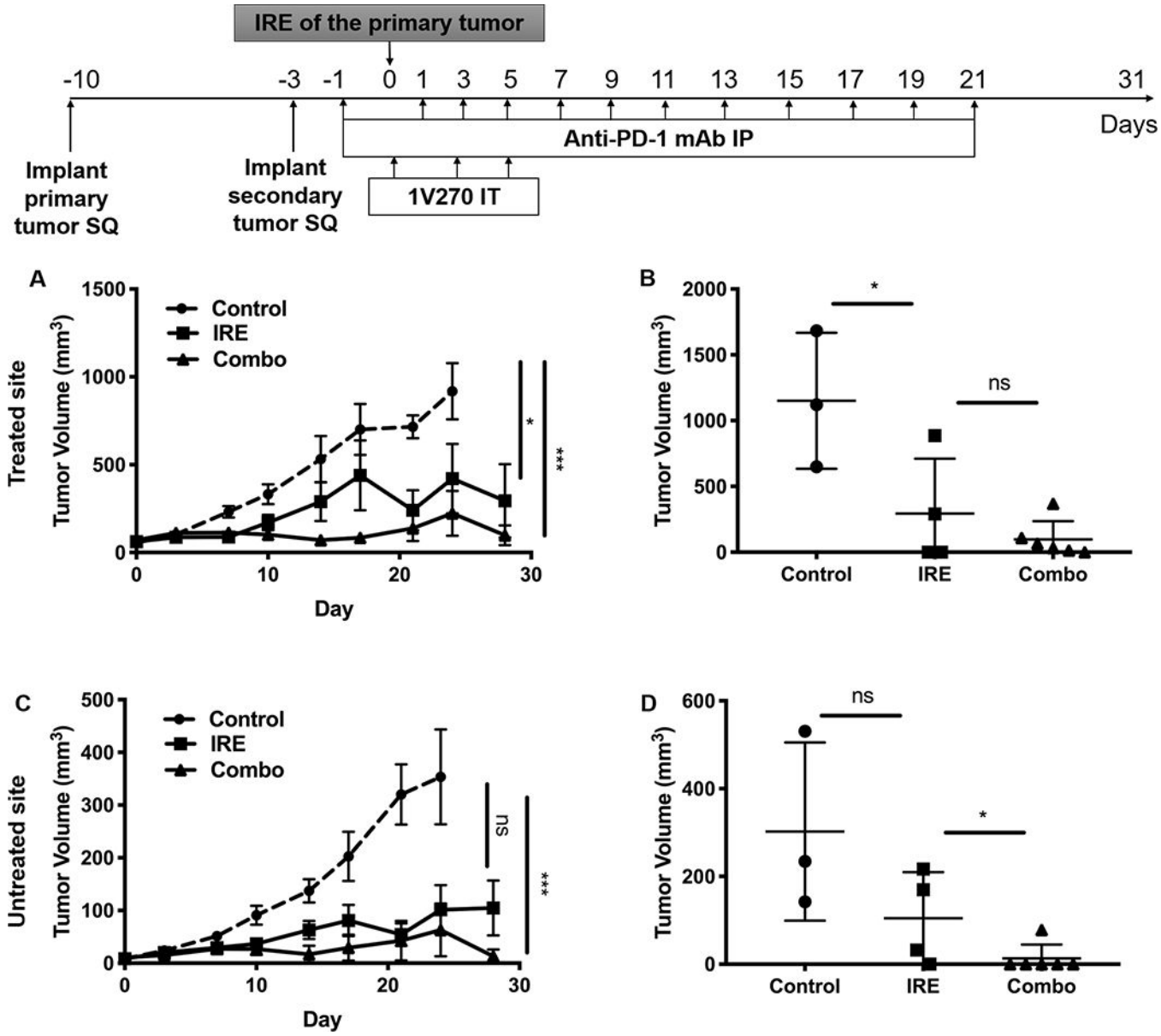


**Figure 6. Combining IRE with both 1V270 and anti-PD1 inhibits the growth of concomitant distant tumors.**

Immunocompetent WT C57BL/6 mice (n=10/group) harboring 2 tumors on opposite flanks were generated by implanting the first tumor with 2.5 X $10^5$ KPC4580P cells in one flank on Day −10 followed by a second tumor on the opposite flank 7 days later (Day −3). IRE was performed on day 0 on the primary larger tumor (Treated site) with the combination treatment given according to the timeline depicted on top. Representative data shown from two independent experiments for tumor growth for the treated site **(A)** and the secondary tumor – untreated site **(C)** with tumor size measurements of individuals represented as dot plots with mean ± SEM on day 28 for the treated site **(B)** and untreated site **(D)** *P < 0.05, **P < 0.01, ***P < 0.001 by two-way ANOVA with post hoc Tukey test (**A and C**) or by one-way ANOVA with post-hoc Bonferroni test (**B and D**); ns – not significant.

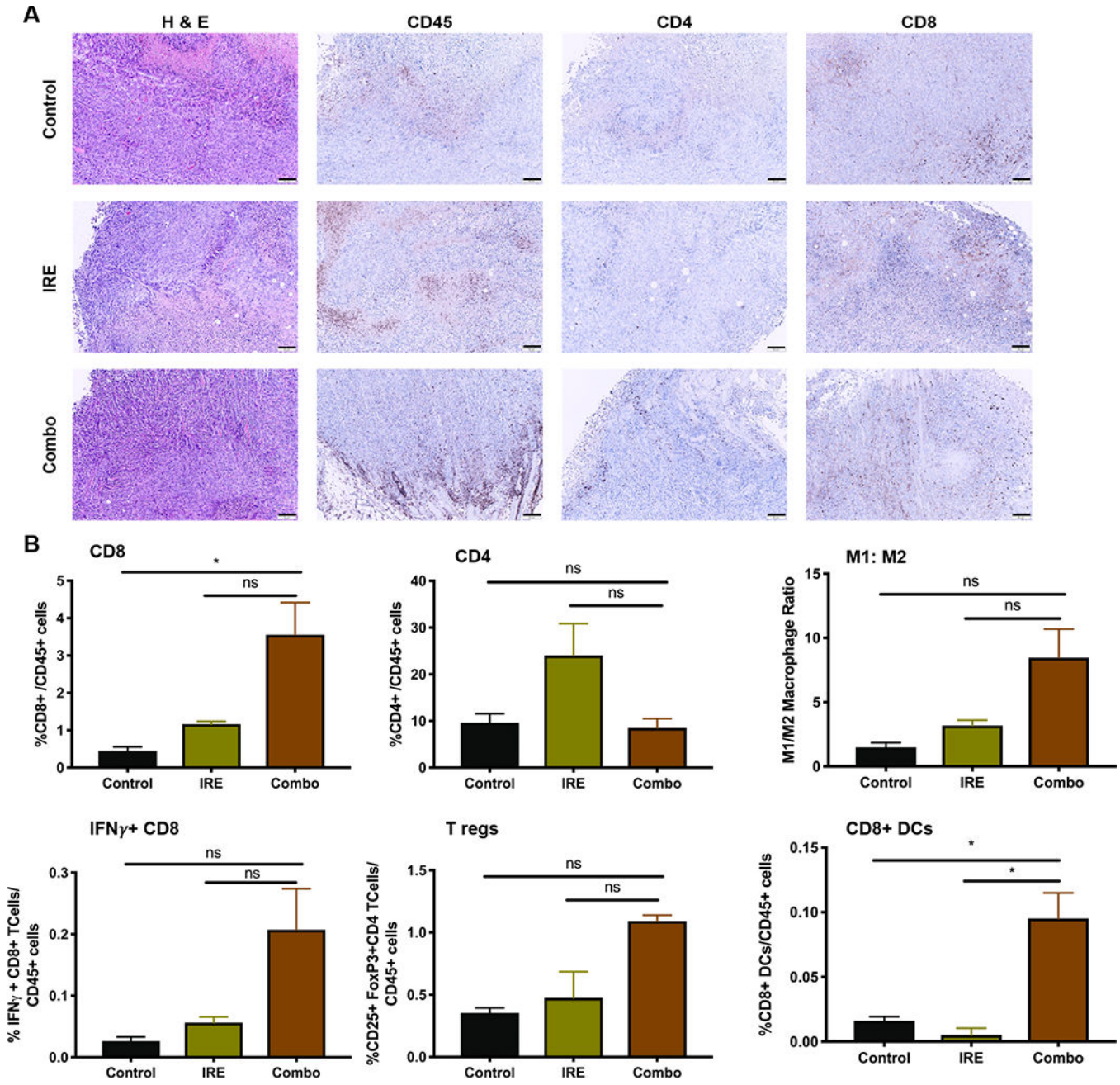


**Figure 7. Immune infiltration in distant untreated tumors is enhanced with the combination of IRE + 1V270 + anti-PD-1 (Combo).**

**(A)** Representative images shown of H & E (panel 1) and IHC (CD45 – Panel 2, CD4 – Panel 3 and CD8 – Panel 4, Blue – nucleus, Brown - antigen) from three tumors. All images taken at 20X magnification; scale bars represent 50 μm. **(B)** Flow cytometric analyses of immune infiltrates performed on day 7 on the untreated tumors (n=3/group). Enhanced immune infiltration and a proinflammatory microenvironment after combination therapy can be observed by the $CD8^+$, $IFN\gamma^+$ $CD8^+$, M1:M2 ratio and $CD8^+$ dendritic cell (DC) graphs

plotted as mean ± SEM. Gating strategy is described in the Supplementary Fig. S6. *P<0.05 by one-way ANOVA with post hoc Bonferroni test; ns – not significant.